Supporting Information

Alkaline-Earth-Metals Regulated Metal Carbides with Bioinspired Gradient OH Spillover for Efficient and Long-Lasting Direct Seawater Electrolysis

Huijuan Wu,[a] Zhenyang Zhao,[a] Mao Wang, [a]* Weiqiong Zheng,[a] Yiming Zhang,[a] Yinghan Wang,[a] Tian Ma,[a] Zhiyuan Zeng,[b] Chong Cheng,[a]* and Shuang Li[a]*

Experimental Procedures

1. Material

$Na_2WO_4 \cdot 2H_2O$, dopamine hydrochloride, HCl, $RuCl_3 \cdot H_2O$, $MgCl_2 \cdot H2O$, $CaCl_2$, $SrCl_2 \cdot H_2O$ and KOH were obtained from Aladdin Co., Shanghai, China. Nafion D520 dispersion was obtained from Alfa Aesar. Unless otherwise stated, all the reagents were of analytical grade and were used as received. The Millipore purification system prepared all aqueous solutions with DI water.

2. Synthesis of catalysts.

Synthesis of DA-WC-Ru Catalysts: First, 2.5 mmol (0.475 g) dopamine hydrochloride (DA) was dissolved in 25 mL water, resulting in a 0.1 M dopamine in water solution. After that, 0.152 mmol $RuCl_3 \cdot H_2O$ were added together into the DA solution and mixed well by stirring. Following, 25 mL sodium tungstate solution (containing 2.5 mmol $Na_2WO_4 \cdot 2H_2O$) was dropped slowly (about 10 min) into the above solution. The reaction happens immediately, then the precipitation starts, and the color of the suspension changes to dark brown during the addition of sodium tungstate; finally, a greenish-yellow precipitate form. The reaction was further stirred for 2 h, and then the product was collected by centrifugation and washed with DI water and ethanol 3 times. The products were dried in an oven at 60 ^oC overnight to obtain this DA-W-Ru precursor.

Synthesis of DA-WC-RuM (M=Mg, Ca, Sr) Catalysts: Dissolve 1 mmol of $MCl_2 \cdot H_2O$ (M=Mg, Ca, Sr) in 50ml of DI water. Then, 0.1g of DA-WC-Ru precursor was placed in the above solution and

stirred for 1h to obtain DA-WC-RuM (M=Mg, Ca, Sr) precursor.

Synthesis of C-WC-RuM (M=Mg, Ca, Sr) Catalysts: Then the DA-WC-RuM precursor was carbonized in an Argon furnace at different temperatures (800^{o}C) for 2 h, with a ramp of 2 ^{o}C/min. The final black powder was donated as C-WC-RuM (M=Mg, Ca, Sr).

Electrochemical Measurements

Ink Preparation: Ink preparation The catalyst ink was prepared by blending the catalyst powder (15 mg) with 100 μL Nafion solution (5 wt. %) and 900 μL ethanol in an ultrasonic bath. 5 μL of catalyst ink was then pipetted onto the GC surface, leading to a catalyst loading of 0.25 mg cm^{-2}. The TOFs data was calculated based on the atomic content (from XPS) of the Ru atom in the catalysts.

Electrodes and Measurements: The electrochemical performance was conducted via Gamry reference 600 workstations (Gamry, USA) with a standard three-electrode system. The electrolytes were fabricated by dissolving 31.17 g KOH (reagent grade, 90%, Aladdin Co.) in 500 mL ultrapure water or simulated seawater. The simulated seawater was prepared by mixing 26.73 g of NaCl, 2.26 g of $MgCl_2$, 3.25 g of $MgSO_2$, 1.12 g of $CaCl_2$, 0.19 g of $NaHCO_3$, 3.48 g of Na_2SO_4, and 0.72 g of KCl in 1 L of ultrapure water. Reversible hydrogen electrode (RHE) is used as the reference, which is placed in a saturated 1.0 M KOH solution that was periodically refreshed to counteract the electrolyte contamination, and the graphite rod is employed as the counter electrode. A glassy carbon rotating disk electrode (RDE) with an area of 0.196 cm^2 served as the substrate for the working electrode to evaluate the hydrogen evolution reaction (HER) activities of various catalysts. The measured HER polarization curves are carried out in an Ar-saturated 1.0 M KOH or simulated seawater electrolyte with a sweep rate of 10 mV s^{-1} at 1600 rpm, which are automatically corrected with real-time iR compensations with a resistance of ~4.4 Ω. The stability tests for the C-WC-Ru, C-WC-RuMg were conducted using the chronopotentiometry method at a current density of 10 mA cm^{-2}. The overall water splitting was performed in a two electrodes cell using carbon cloth (CC) as electrode at dimensions of 1.0 × 1.0 cm^2 with a catalyst loading of 1.0 mg cm^{-2}.

To prepare the electrodes, CC was rinsed with acetone, ethyl alcohol, and water in an ultrasonic bath for 20 min, respectively. Subsequently, the CC was submerged in a 2 M H_2SO_4 solution for another 12 h. Afterward, the electrode was dried in a vacuum oven at 60 ° C for 30 min and then coated with 100 μ L of prepared catalysts ink with a concentration of 10.0 mg mL^{-1}. Before measuring, the

electrodes were first moistened by dipping in a mixture of ethanol and water (50:50 v/v), then multiple times in electrolyte.

Electrochemical impedance spectroscopy (EIS) was performed using a potentiostatic EIS method from 100 KHz to 0.1 Hz with a 37 mV AC potential at 1600 rpm. The chronopotentiometry method obtained the long-term durability of all the samples are conducted without real-time iR calibration. The mass activity was calculated based on the following equation: Mass activity = I/m, where I (A) is the measured current, m (mg) is the mass of Ru loaded on the glassy carbon electrode. The turnover frequency (TOF) is calculated based on the following equation: TOF = I/2nF, where I (A) is the measured current. F is the Faraday constant (96485 C mol^{-1}). n = m/M, n is the number of Ru active sites (mol) loaded on the glassy carbon electrode, m is the mass of Ru, and M is the atomic mass. The ECSA for electrode was estimated from electrochemical C_{dl} of catalytic surface. The specific capacitance for a flat surface is generally found to be in the range of 20 ~ 60 μF cm^{-2}. Assume that the specific capacitance of a flat surface is ~ 40 μF cm^{-2} for 1 cm^2 of real surface area. The following formula is used to calculate ECSA: ECSA = Specific capacitance (mF cm^{-2}) 40 μF cm^{-2} per cm^2. The long-term durability of all the samples obtained by chronopotentiometry method are conducted without real-time iR calibration.

Local pH test on electrocatalyst surface: We used rotating ring-disk electrode (RRDE) technique (ChemElectroChem., 2019, 6, 4750; Nat. Energy, 2023, 8, 264) to quantitatively detect local pH on the C-WC-RuMg and carbon support surfaces at different applied potentials in neutral PBS solution. According to convective-diffusion equation of Albery et al (J. Chem. Soc. Faraday Trans. 1983, 79, 2583), the principle of the RRDE technology is based on the relationship between the pH values of the disk surface and the ring surface in solutions with arbitrary pH (Figure 2a). The calculation formula is as follows:

$$c_{rt,\,H+}\text{-}c_{rt,\,OH-} = N_D(c_{d,\,H+}\text{-}c_{d,\,OH-})+(1\text{-}N_D)(c_{\infty,\,H+}\text{-}c_{\infty,\,OH-}) \qquad (1\text{-}1)$$

where $c_{rt,\,H+}$ and $c_{d,\,H+}$ are the concentrations of H^+ on the RE and DE, respectively, $c_{rt,\,OH-}$ and $c_{d,\,OH-}$ are the concentrations of OH^- on the RE and DE, respectively, $c_{\infty,\,H+}$ and $c_{\infty,\,OH-}$ are the concentrations of H^+ and OH^- in the bulk electrolyte, respectively, and N_D = 0.37 is the collection efficiency of the RE. Then, the pH dependence of the open circuit potential (E_{ocp}) in PBS solution was measured with Pt RE. Because in the H_2-saturated solution with inert electrolyte, the OCP of the Pt electrode would indicate the equilibrium potential (E) of $2H^+ + 2e^- \rightarrow H_2$, which varies with pH according to the Nernst

equation:

$$E\ (V\ vs.\ SHE) = (-2.303RT/F)\ pH \qquad (1\text{-}2)$$

The fugacity of H_2 is assumed to be equal to unity and R, T and F are the gas constant, the absolute temperature, and the Faraday constant. Hence, the relationship between the disk pH and the ring pH can be corroborated experimentally. To confirm that the OCP of the Pt ring electrode accurately reflects the hydrogen equilibrium potential, the ring OCPs were measured with solutions of various pH values without any reactions at the disk electrode at room temperature (~ 20 ^{o}C). The time dependence of the ring OCP is shown in Figure S38. The pH values shown in the figure are those in the bulk solution measured by a pH meter. Each OCP showed good stability. These OCPs were plotted against the pH values in (1-3), where the dotted line obeys the Nernst equation. The ring responses to the change in pH were in good agreement with the Nernst equation.

$$E = -0.05834pH - 0.21011 \qquad R^2 = 0.994 \qquad (1\text{-}3)$$

Next, the local pH measurement was performed on the C-WC-RuMg and carbon support in neutral pH solution during HER. A solution of H_2-saturated 1.0 M PBS was used as an electrolyte. The bulk pH of the solution is 7.

To obtain steady-state local pH value, constant potential method was performed on the disk electrode, and OCP was measured simultaneously on the Pt ring electrode. In the constant potential method, each potential is maintained for 200 s (E = -0.1, -0.2, -0.3, -0.4, -0.5, and -0.6 VRHE) to obtain a steady-state current response (j). All measurements were carried out at rotation speed of 1600 rpm at room temperature.

The relatively smooth i-t curves indicates that the electrode surface is in steady state at different potentials (Figure S38a). The measured local pH on cathode surfaces (C-WC-RuMg and carbon) are shown in Figure 1c. For the C-WC-RuMg support, the pH of the catalyst surface will be from 7.69 to 9.58 as the potential is reduced from 0.1 to -0.6 V_{RHE}, which undoubtedly confirms its local alkaline microenvironment. In sharp contrast, the pH of carbon cathode surface is from 7.75 to 8.63 in range of 0.1 ~ -0.6 V_{RHE}. Astonishingly, when the bias (-0.6 V_{RHE}) is removed, the surface of C-WC-RuMg and carbon cathodes turn back to steady neutral states, respectively.

Characterizations

The scanning electron microscopy (SEM) was performed with Apreo S HiVac-ThermoFisherScientific

(FEI). The N_2 adsorption/desorption isotherms were obtained by the Autosorb iQ and based on the Brunauer-Emmett-Teller (BET) to assess the surface area. All powder samples were degassed at 150 °C overnight prior to the actual measurement. The pore size distribution (PSD) plots were obtained from the adsorption branch of the isotherms based on the QSDFT model. The X-ray diffraction (XRD, Ultima IV (Rigaku, Japan)) was used to analyze crystal structures of the catalysts with Cu Kα radiation for a 2θ range of 10-80°. The surface elemental composition and all binding energies were measured by X-ray photoelectron spectroscopy (XPS, Thermo ESCALAB 250Xi) with Al Kα monochromatic X-ray sources, and results were analyzed via the Thermo Scientific Avantage software to confirm the surface chemical structures and metal contents. X-ray absorption spectra (XAS) were collected on the beamline BL07A1 in NSRRC (National Center for Synchrotron Radiation Research). The radiation was monochromatized by scanning a Si (111) double-crystal monochromator. Samples were pressed into thin slices and positioned at 90° to the incident beam in the sample holder. X-ray absorption near-edge structure (XANES) and extended Xray absorption fine structure spectra (EXAFS) data reduction and analysis were processed by Athena software. The X-ray diffraction patterns were used to analyze crystal structures of the catalysts via a Bruker D8 Focus X-ray diffractometer with Cu Kα radiation for a 2θ range of 10-80°, which were analyzed by MDI Jade and Origin. For aberration-corrected STEM analysis, the sample was dop-casted on Lacey carbon-coated Cu grids. STEM investigations were performed on a JEOL JEM-ARM 200F scanning transmission electron microscope equipped with a cold field emission electron source.

Molecular dynamics simulation

All-atomic molecular model was constructed to explore the effect of alkaline-earth-metal atom doping. As illustrated in Figure 1d-f, the Mg-doped materials C-WC-RuMg electrocatalysts were placed at the bottom of the simulation box. A water bulk that contains 28 OH^- and 28 Na^+ ions was above the doped surface. Four different simulation systems were built including no-doping and Mg-doping at different sites. The whole simulation is about 4.6×4.0×10 nm^3. Periodic boundary conditions were applied to all three directions. The electrocatalysts were assumed to be rigid with nonbonding interactions $\sum 4\varepsilon_{ij}\left[\left(\frac{\sigma_{ij}}{r_{ij}}\right)^{12}-\left(\frac{\sigma_{ij}}{r_{ij}}\right)^{6}\right]+\sum\frac{q_i q_j}{4\pi\varepsilon_0 r_{ij}}$, where ε_{ij} and σ_{ij} are the well and collision diameter of Lennard-Jones (LJ) potential, r_{ij} is the distance between atom *i* and *j*, q_i is the atomic charges of atom

i, and ε_0 is the permittivity of vacuum. The LJ potential parameters were adopted from the universal force field (UFF)[1]. The atomic charges of the electrocatalysts were generated using DDEC atomic charge. [2] Water was modeled by the TIP3P model [3] and the Na^+ ions were described by the CHARMM force field. [4]

The electrostatic interactions were calculated with the Particle-Mesh Ewald method, while the LJ interactions were calculated using a cutoff of 1.2 nm. The temperature was maintained at 300 K using v-rescale scheme and the time step was 1 fs. After equilibration, constant number of particles, volume, and temperature (NVT) ensemble was used for output simulation. The NVT simulation duration was 40 ns. All the MD simulations were performed using GROMACS 2021 [5] and the model was visualized by VMD 1.9 [6]. For OH^-, Cl^- density calculation, the probability density was calculated using ions within 5 A of the catalyst surface.

Supplementary Figures.

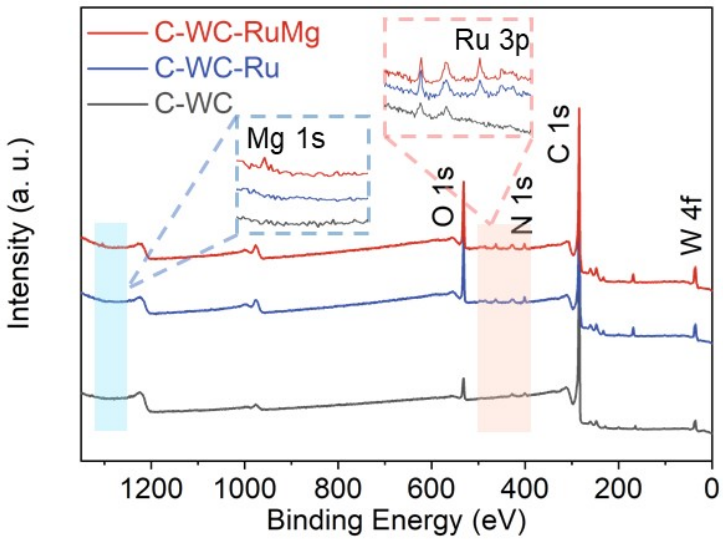

Figure S1. a) XPS survey spectra for C-WC-RuMg.

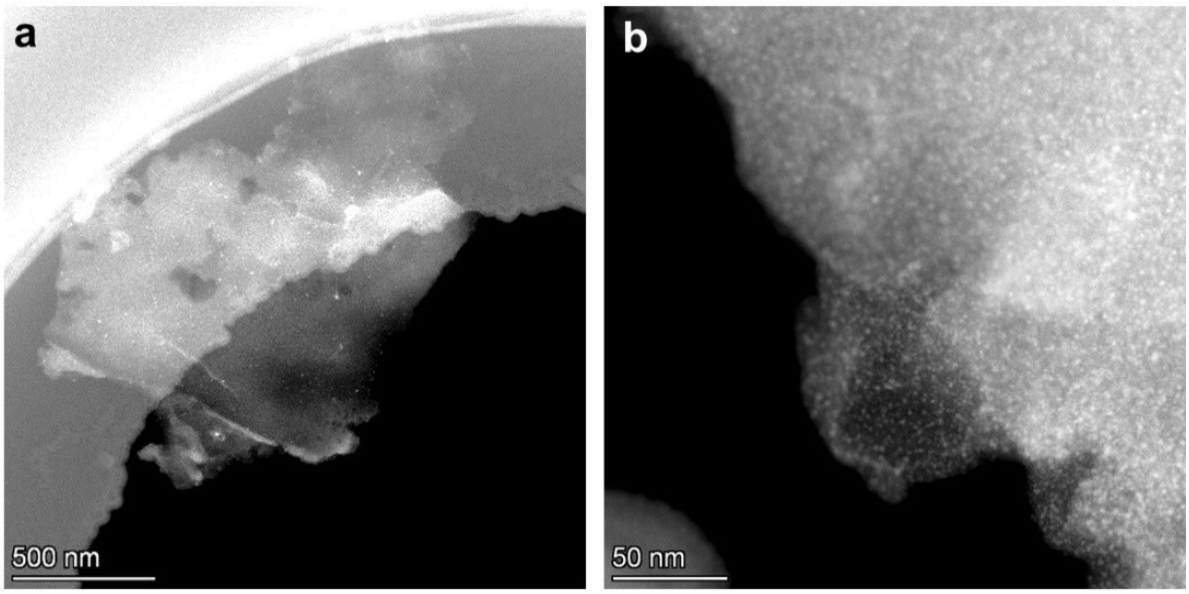

Figure S2. STEM image of C-WC-RuMg in different magnification.

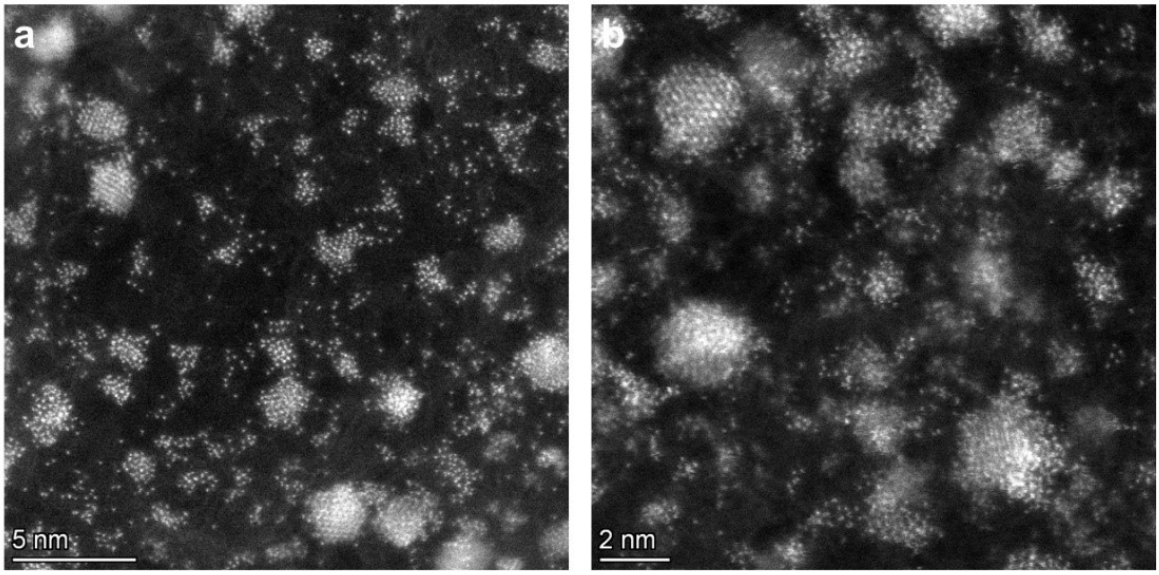

Figure S3. HAADF-STEM images of C-WC-RuMg at different magnifications

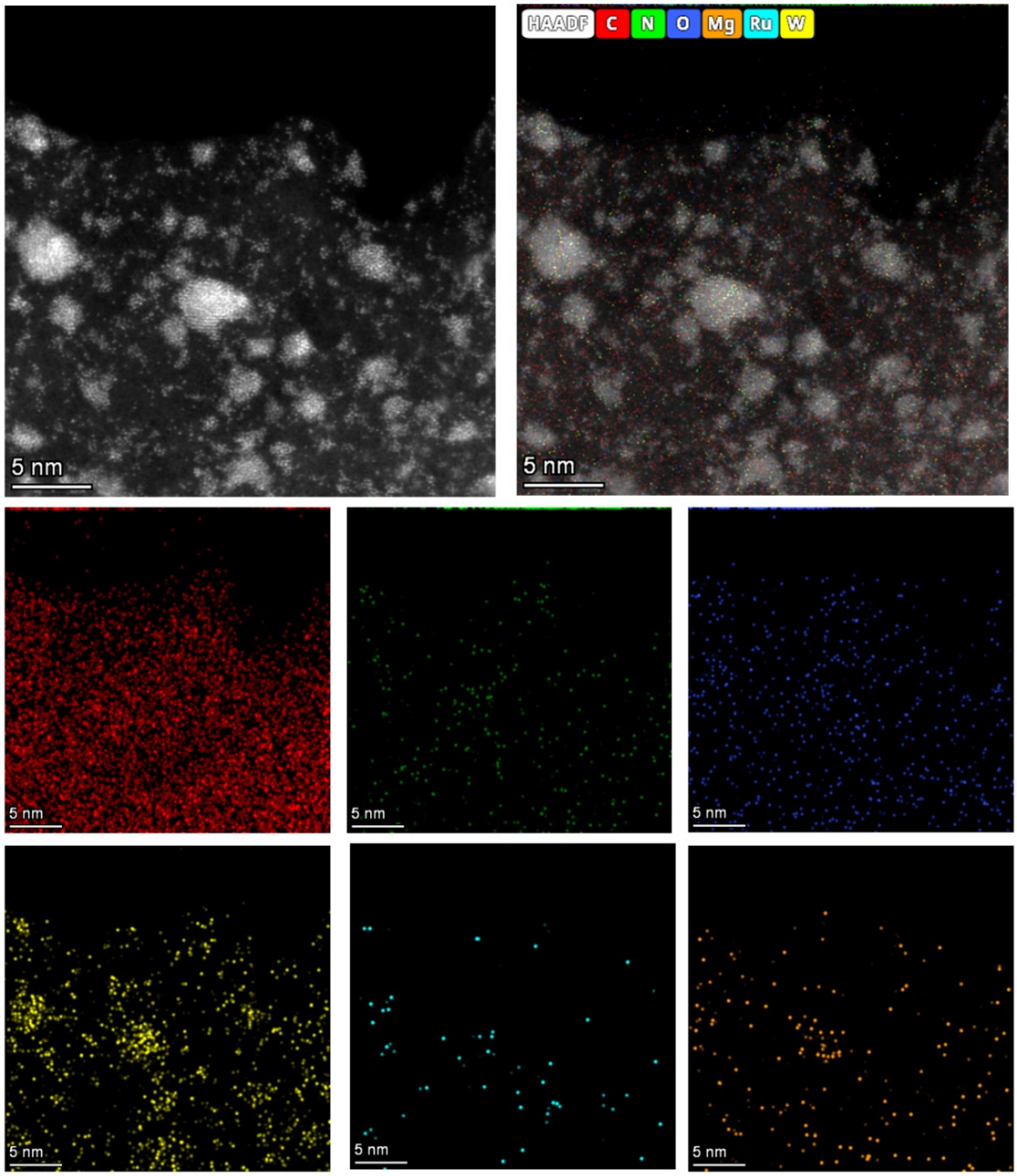

Figure S4. EDS mapping of C-WC-RuMg in HAADF-STEM images.

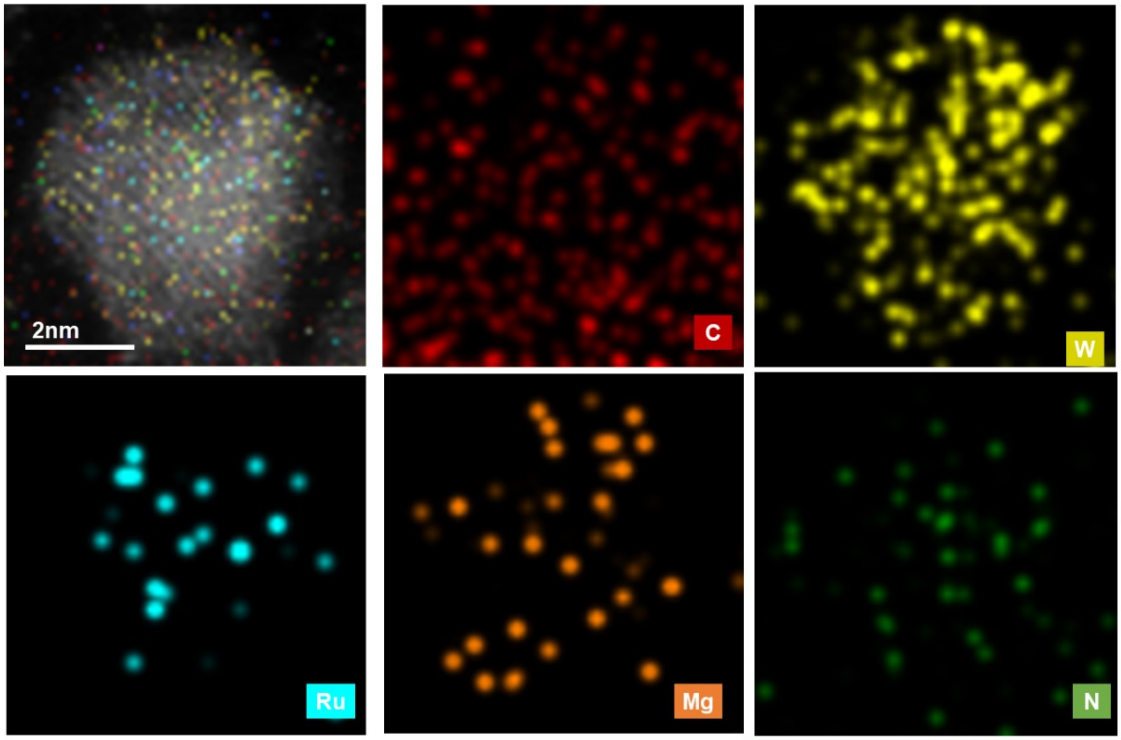

Figure S5. EDS mapping of C-WC-RuMg in HAADF-STEM images.

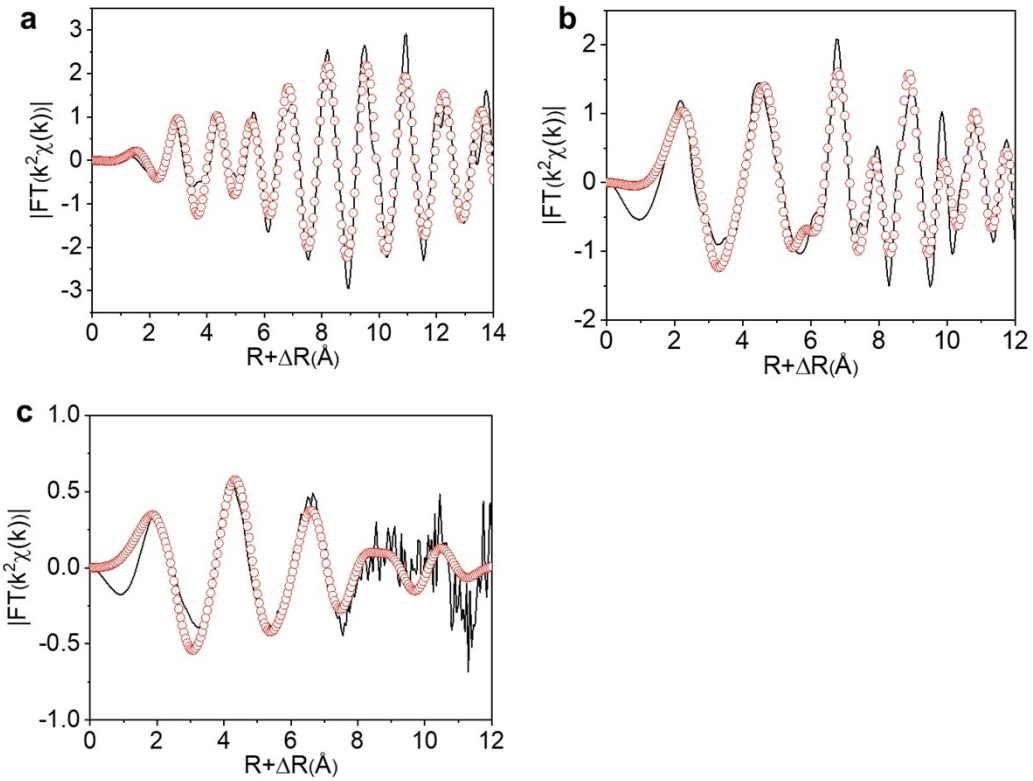

Figure S6. k^2-weight FT-EXAFS fitting curves of a,b) Ru foil, c,d) RuO_2, and e,f) C-WC-RuMg.

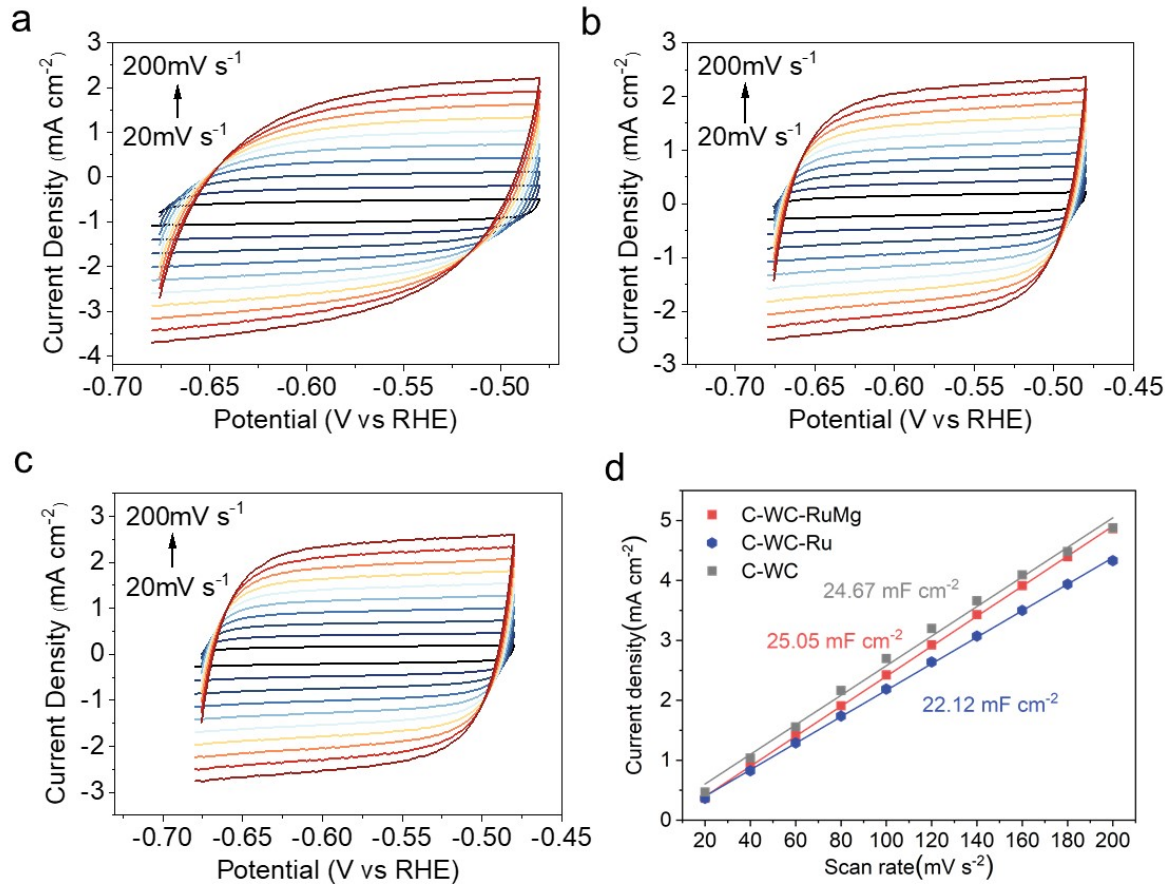

Figure S7. The CV curve of a) C-WC, b) C-WC-Ru, and c) C-WC-RuMg. d) the calculated C_{dl}.

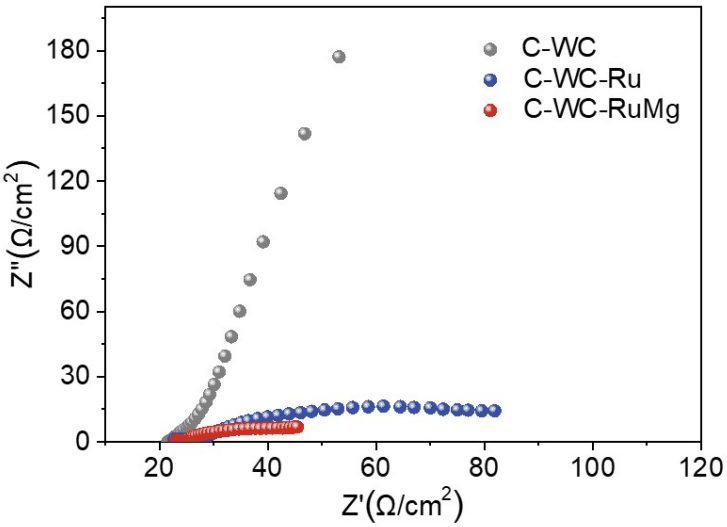

Figure S8. The electrochemical impedance spectroscopy (EIS) of the as-synthesized catalysts. The Nyquist plot of different catalysts at the overpotential of 200 mV.

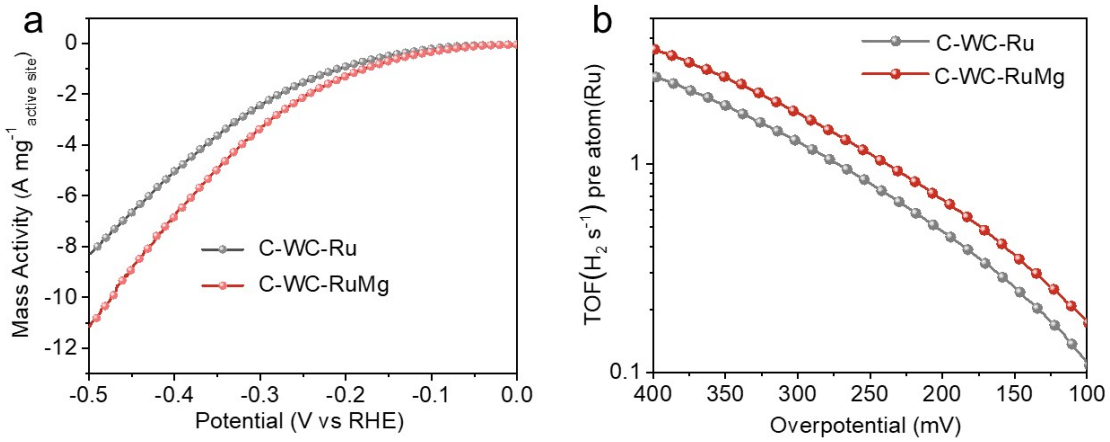

Figure S9. Mass activity and TOF values of C-WC-Ru and C-WC-RuMg based on Ru content from XPS.

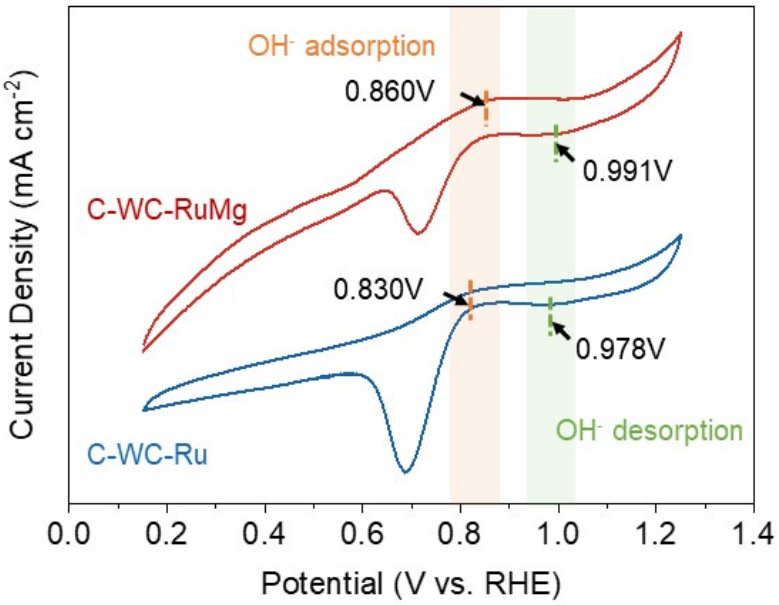

Figure S10. The CV curve for C-WC-Ru and C-WC-RuMg at the scan rate of 20 mV s^{-1}.

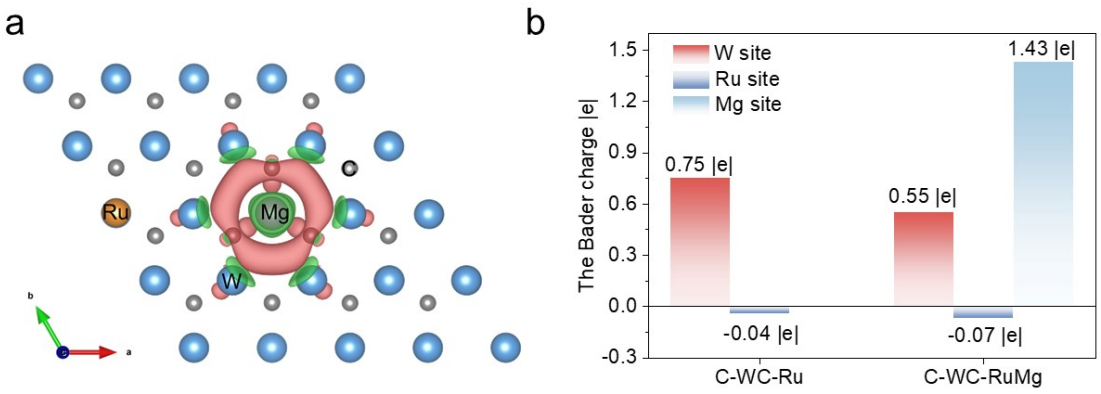

Figure S11. a) the differential charge and **b)** Bader charge |e| of individual metal sites in C-WC-RuMg.

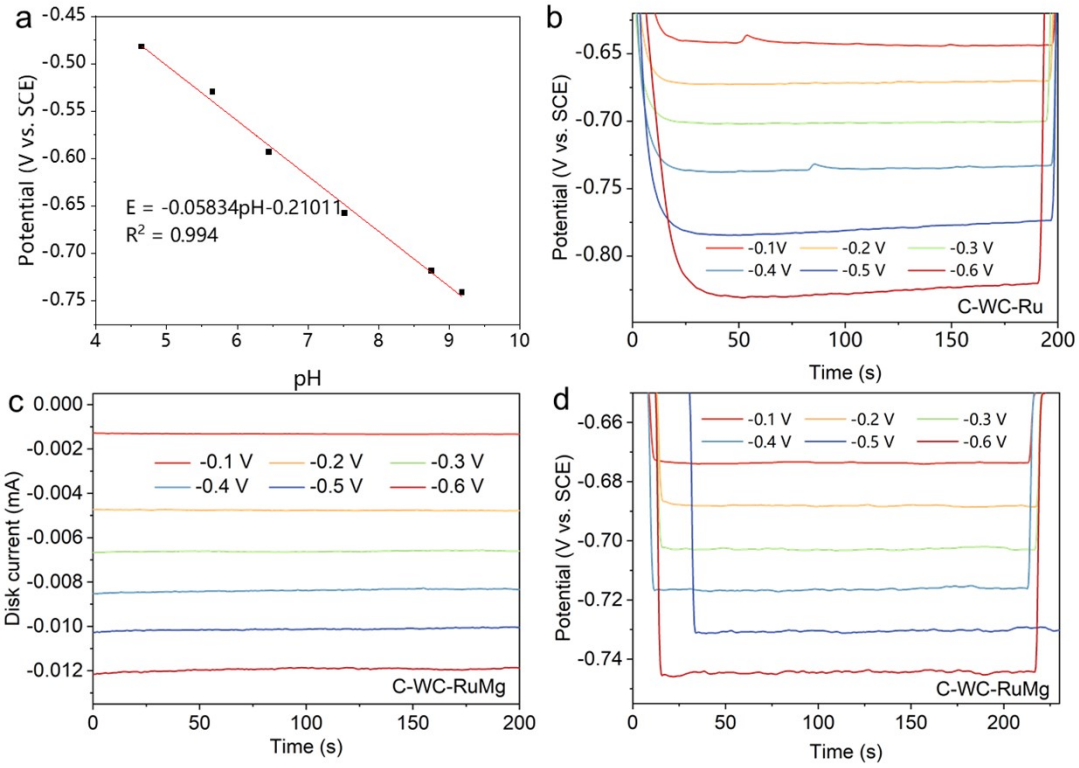

Figure S12. a) pH dependence of open circuit potential (Eocp) for Pt-ring electrode. The measurement was performed in PBS solutions, and the pH of the PBS solutions was changed by adding H_2SO_4 or KOH. b) and d) Measure OCP of ring. c) i-t plots of C-WC-RuMg in different potentials.

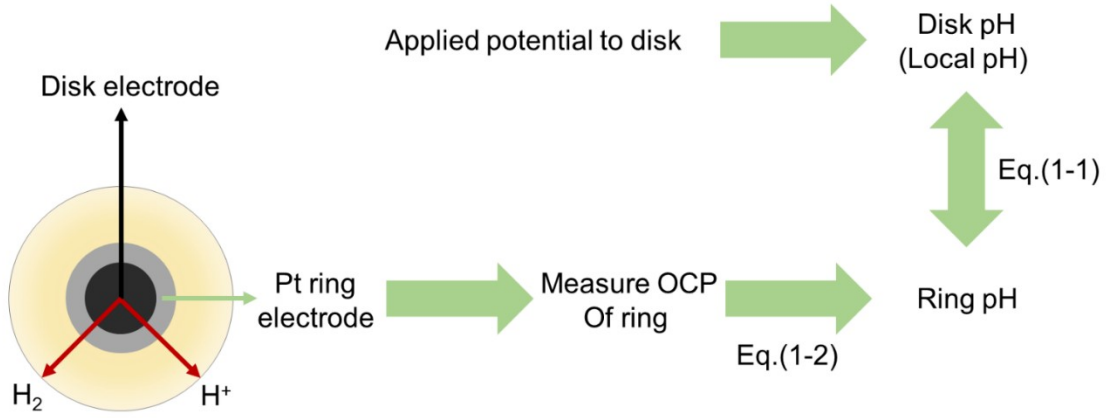

Figure S13. Principles for detecting local pH. Schematic diagram for monitoring pH on the electrode surface using an RRDE technology, the equations (1-2) and (1-3) are given in Method section.

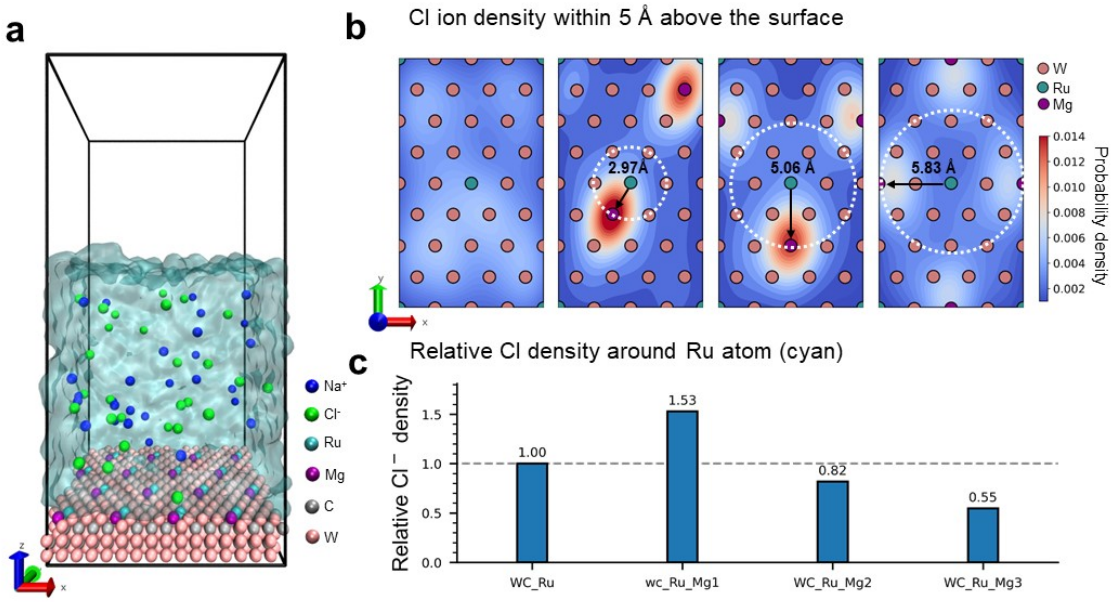

Figure S14. Molecular dynamics simulation. a) Modeling of Cl^- adsorption from seawater by Mg atoms in C-WC-RuMg. b) The density of Cl^- within 5 Å above the surface. c) Relative the density of Cl^- near Ru (compare to no alkaline earth metal).

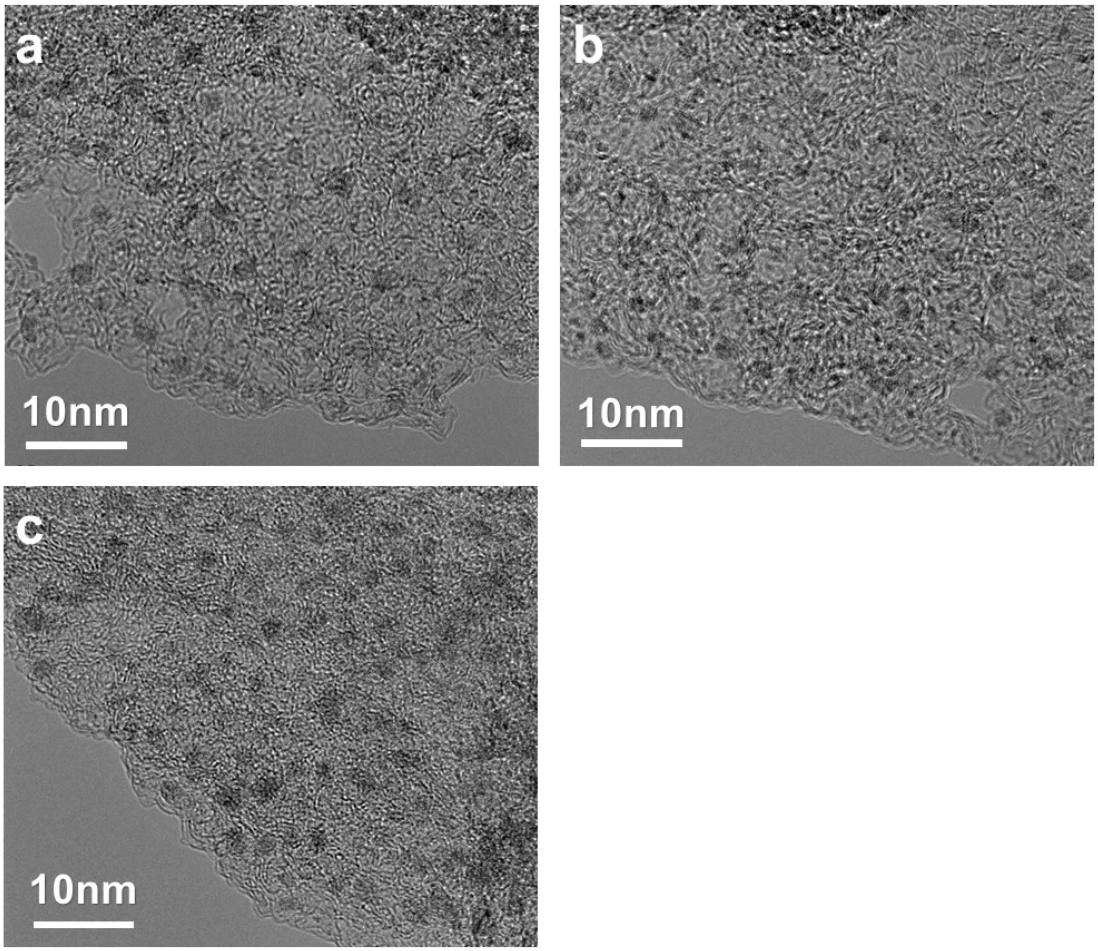

Figure S15. a-c) TEM image of C-WC-RuM(M=Mg, Ca, Sr).

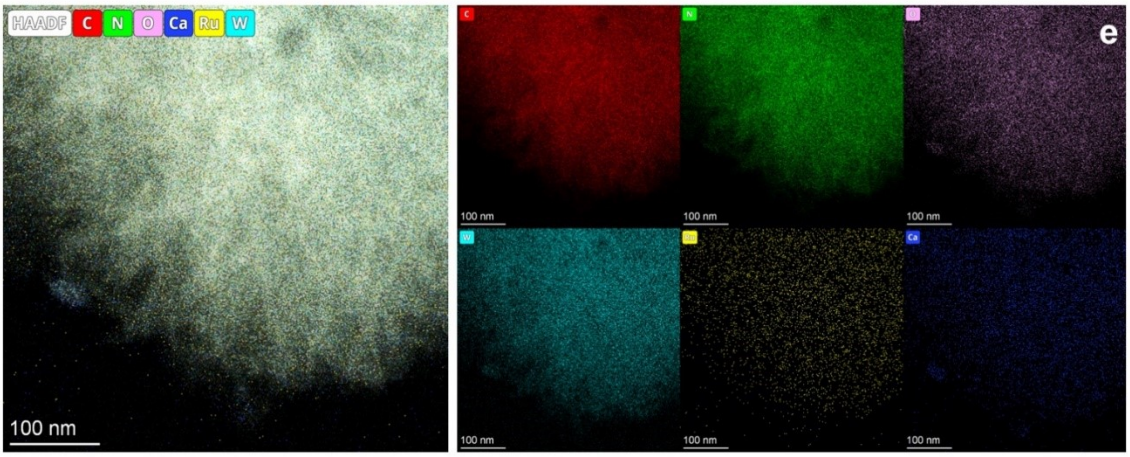

Figure S16. TEM image and EDS of C-WC-RuCa.

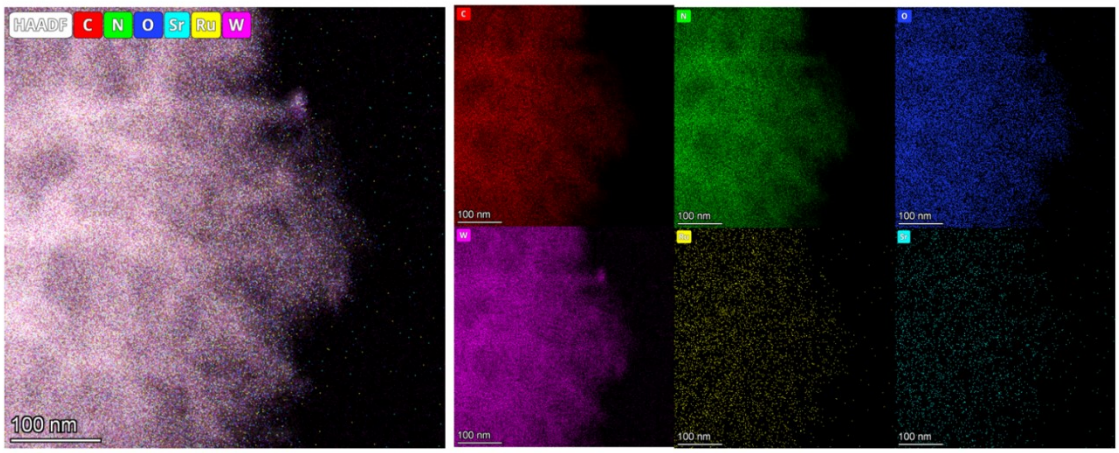

Figure S17. TEM image and EDS of C-WC-RuSr.

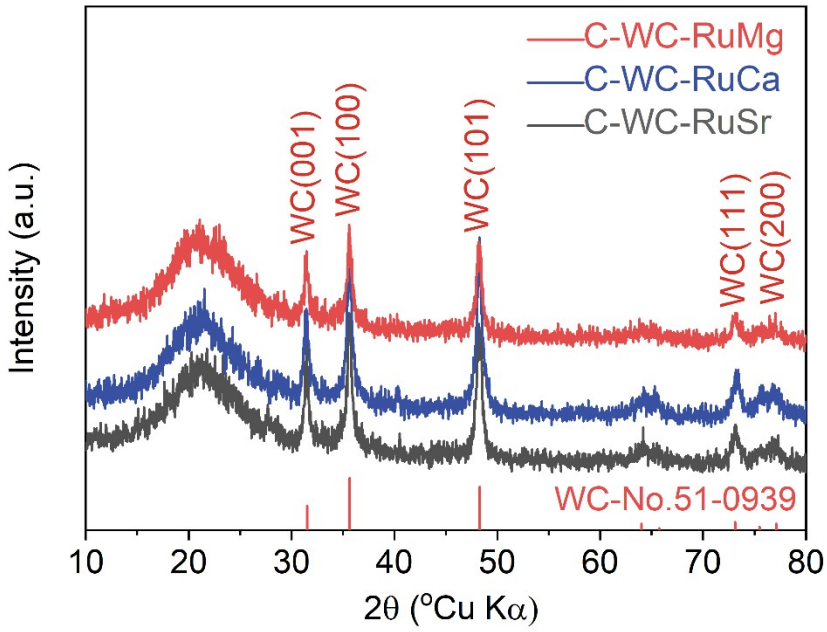

Figure S18. XRD of C-WC-RuM(M=Mg, Ca, Sr).

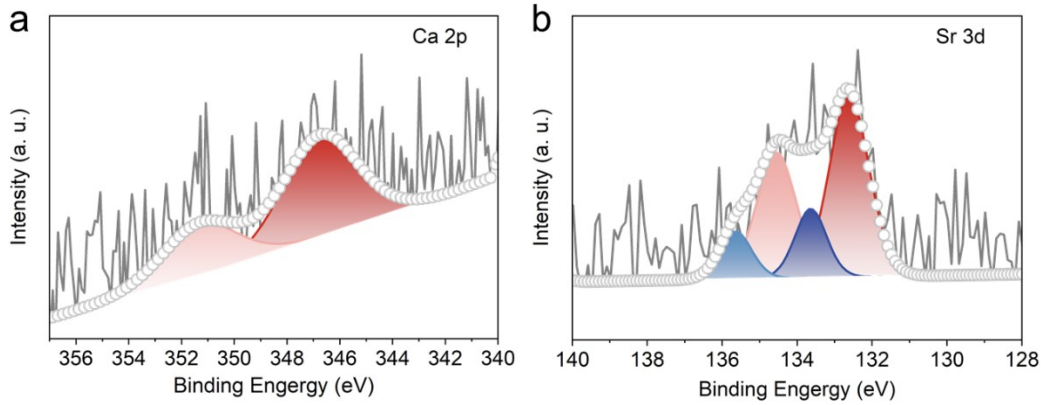

Figure S19. a) The Ca 2p XPS spectrum of C-WC-RuCa and a) the Sr 3d XPS spectrum of C-WC-RuSr.

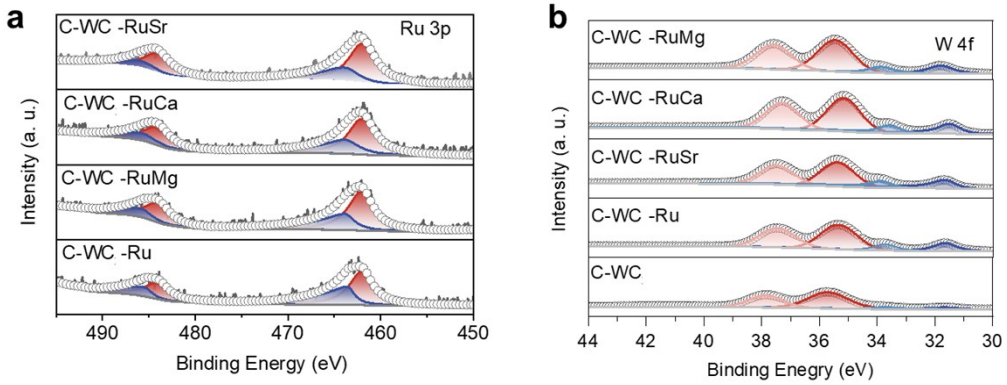

Figure S20. The high resolution of a) Ru 3p and b) W 4f XPS spectra for C-WC, C-WC-Ru, C-WC-RuM (M=Mg, Ca, Sr).

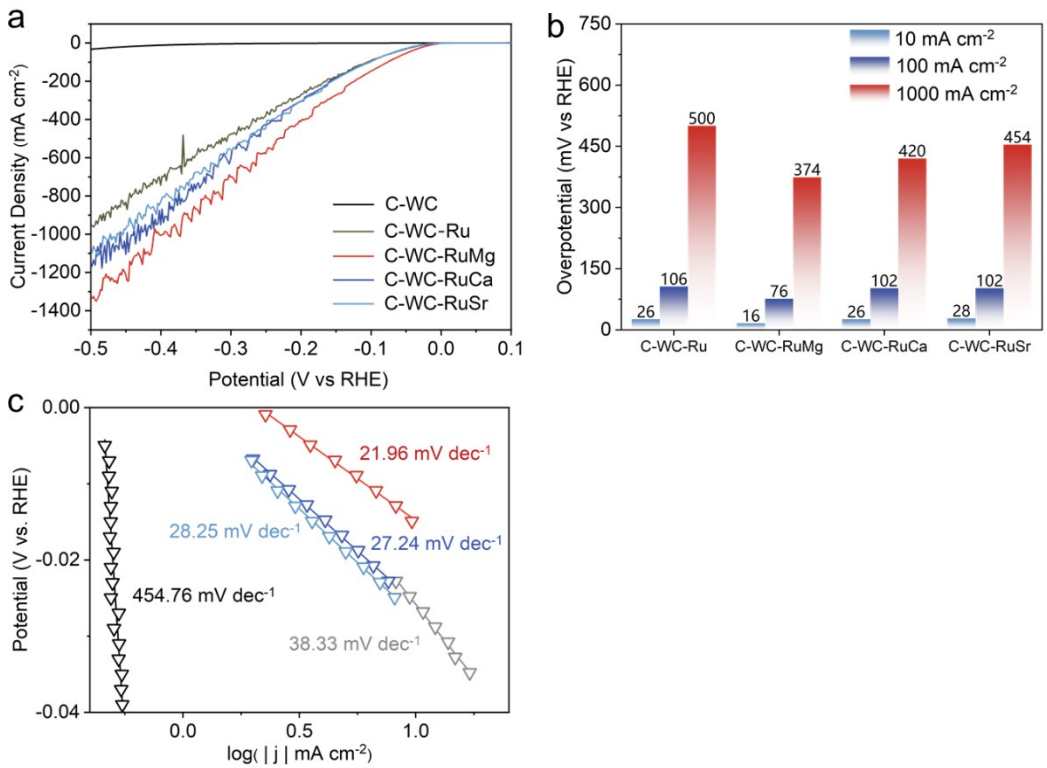

Figure S21. a) The LSV curve, b) overpoterntial value, ane c) Tafel of C-WC, C-WC-Ru, C-WC-RuM (M=Mg, Ca, Sr) in 1M KOH.

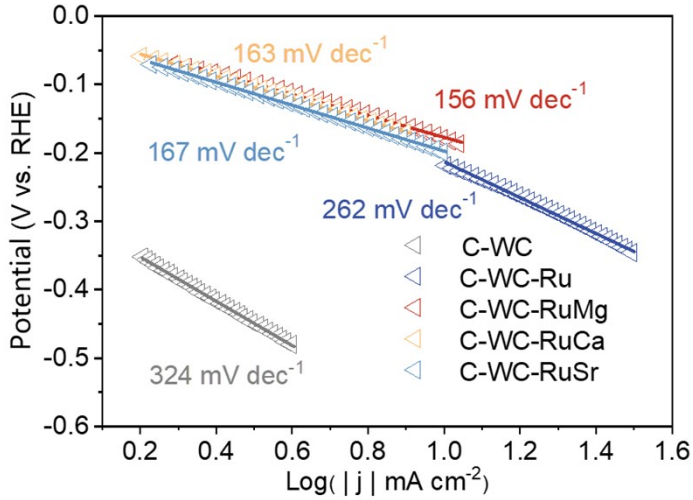

Figure S22. Electrocatalytic HER performance in seawater. Tafel slopes of C-WC, C-WC-Ru, and C-WC-RuM (M=Mg, Ca, Sr) at a scan rate of 5 mV s^{-1}.

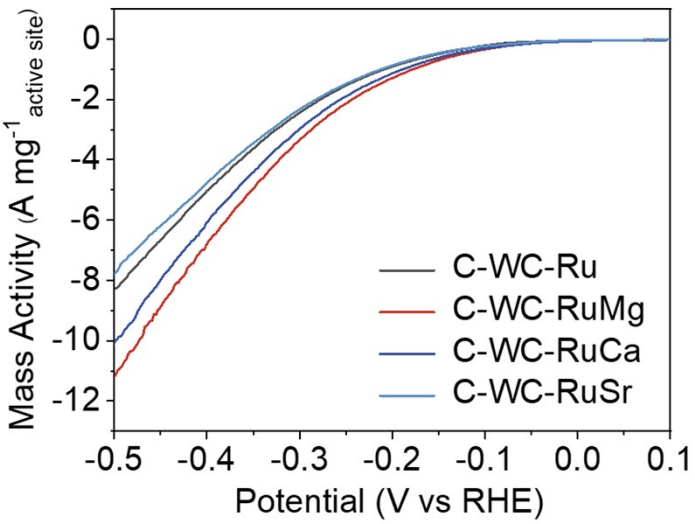

Figure S23. Mass activities of the catalysts on the basis of Ru atoms.

Table S1. The percent mass of the element of C, N, O, W, Ru, and M (M=Mg, Ca, Sr) in the synthesized catalysts by XPS tests.

	C (wt %)	N (wt %)	O (wt %)	W (wt %)	Ru (wt %)	Mg/Ca/Sr (wt %)
C-WC	91.92	1.72	5.79	0.56		
C-WC-Ru	68.20	2.10	15.76	10.40	3.54	
C-WC-RuSr	63.69	2.38	15.84	12.88	4.60	0.61
C-WC-RuCa	61.48	2.54	16.42	15.01	3.92	0.62
C-WC-RuMg	64.35	2.08	15.68	13.43	3.91	0.55

Table S2. Elemental contents of W, C, O, N, Fe, and Ni in the synthesized catalysts by XPS tests.

	C (at %)	N (at %)	O (at %)	W (at %)	Ru (at %)	Mg/ Ca/ Sr (at %)
C-WC	91.92	1.72	5.79	0.56		
C-WC-Ru	81.24	2.17	14.27	0.82	0.51	
C-WC-RuSr	80.52	2.58	15.04	1.06	0.69	0.10
C-WC-RuCa	79.20	2.81	15.88	1.26	0.60	0.24
C-WC-RuMg	80.92	2.24	14.81	1.10	0.58	0.34

Table S3. EXAFS fitting parameters at the Ru K-edge for various samples.

Sample	Shell	N	R(Å)	σ^2x10^2 ($Å^2$)	$\triangle E_0$ (eV)	R-space rang(Å)	R-factor(%)
Ru Foil	Ru-Ru	12.00	2.67	0.4	6.55	2.70	0.018
	Ru-O	6.44	1.97	0.24	2.65	1.98	
RuO_2	Ru-Ru	6.54	3.16	0.63	2.65	3.11	0.018
	Ru-Ru	3.03	3.56	0.17	2.65	3.53	
C-WC-RuMg	Ru-O/C	3.84	2.00	0.68	7.809	2.01	0.018
	Ru-W	0.89	2.788	0.99	7.809	2.82	

N: coordination numbers; R: bond distance; $\sigma^2\times10^2$: Debye-Waller factors; ΔE_0: the inner potential correction. R factor: goodness of fit. S_0^2 was set to 0.816, according to the experimental EXAFS fit of Ru foil by fixing CN as the known crystallographic value.

References

[1] A. K. Rappé, C. J. Casewit, K. Colwell, W. A. Goddard III, W. M. Skiff, *Journal of the American chemical society* **1992**, *114*, 10024-10035.

[2] N. G. Limas, T. A. Manz, *RSC advances* **2018**, *8*, 2678-2707.

[3] W. L. Jorgensen, J. Chandrasekhar, J. D. Madura, R. W. Impey, M. L. Klein, *The Journal of chemical physics* **1983**, *79*, 926-935.

[4] A. D. MacKerell Jr, B. Brooks, C. L. Brooks III, L. Nilsson, B. Roux, Y. Won, M. Karplus, *Encyclopedia of computational chemistry* **2002**, *1*.

[5] M. J. Abraham, T. Murtola, R. Schulz, S. Páll, J. C. Smith, B. Hess, E. Lindahl, *SoftwareX* **2015**, *1*, 19-25.

[6] W. Humphrey, A. Dalke, K. Schulten, *Journal of molecular graphics* **1996**, *14*, 33-38.

[7] a) Q. Zhang, Z. L. Zhe Ru, R. Daiyan, P. Kumar, J. Pan, X. Lu, R. Amal, *ACS Appl. Mater. Interfaces* **2021**, *13*, 53798-53809; b) H. Jin, X. Liu, A. Vasileff, Y. Jiao, Y. Zhao, Y. Zheng, S.-Z. Qiao, *ACS Nano* **2018**, *12*, 12761-12769; c) Y. Liu, X. Hu, B. Huang, Z. Xie, *ACS Sustainable Chem. Eng.* **2019**, *7*, 18835-18843; d) L. Xiu, W. Pei, S. Zhou, Z. Wang, P. Yang, J. Zhao, J. Qiu, *Adv. Funct. Mater.* **2020**, *30*, 1910028; e) M. Hu, H. Chen, B. Liu, X. Xu, B. Cao, P. Jing, J. Zhang, R. Gao, J. Zhang, *Appl. Catal., B* **2022**, *317*, 121774; f) C. Yang, L. Zhou, C. Wang, W. Duan, L. Zhang, F. Zhang, J. Zhang, Y. Zhen, L. Gao, F. Fu, Y. Liang, *Appl. Catal., B* **2022**, *304*, 120993; g) X. Bu, X. Liang, Y. Bu, Q. Quan, Y. Meng, Z. Lai, W. Wang, C. Liu, J. Lu, C.-M. Lawrence Wu, J. C. Ho, *Chem. Eng. J.* **2022**, *438*, 135379; h) G. Liu, H. Lv, Q. Quan, X. Li, H. Lu, W. Li, X. Cui, L. Jiang, *Chem. Eng. J.* **2022**, *450*, 138079; i) Y. Luo, P. Wang, G. Zhang, S. Wu, Z. Chen, H. Ranganathan, S. Sun, Z. Shi, *Chem. Eng. J.* **2023**, *454*, 140061; j) Y. Yao, Y. Zhu, C. Pan, C. Wang, S. Hu, W. Xiao, X. Chi, Y. Fang, J. Yang, H. Deng, S. Xiao, J. Li, Z. Luo, Y. Guo, *J. Am. Chem. Soc.* **2021**, *143*, 8720-8730; k) Y. Xu, H. Lv, H. Lu, Q. Quan, W. Li, X. Cui, G. Liu, L. Jiang, *Nano Energy* **2022**, *98*, 107295; l) J. Li, M. Song, Y. Hu, C. Zhang, W. Liu, X. Huang, J. Zhang, Y. Zhu, J. Zhang, D. Wang, *Nano Res.* **2022**, *16*, 3658-3664; m) L. Wang, Y. Hao, L. Deng, F. Hu, S. Zhao, L. Li, S. Peng, *Nat. Commun.* **2022**, *13*, 5785; n) J. Jian, H. Kang, D. Yu, X. Qiao, Y. Liu, Y. Li, W. Qin, X. Wu, *Small* **2023**, *19*, 2207378; o) D. Wu, D. Chen, J. Zhu, S. Mu, *Small* **2021**, *17*, 2102777.